Electronic Supplementary Material (ESI) for Journal of Materials Chemistry B.

Supplementary Information

Injectable *in situ* gelling methylcellulose-based hydrogels for bone tissue regeneration

Lorenzo Bonetti,[a] Silvia Borsacchi, *[b,c] Alessandra Soriente,[d] Alberto Boccali,[a] Lucia Calucci,[b,c] Maria Grazia Raucci[d] and Lina Altomare *[a,e]

[a.] Department of Chemistry, Materials, and Chemical Engineering "G. Natta", Politecnico di Milano, Piazza Leonardo da Vinci 32, 20133, Milano, Italy.
[b.] Institute for the Chemistry of the Organometallic Compounds (ICCOM), Italian National Research Council (CNR), Via G. Moruzzi 1, 56124 Pisa, Italy.
[c.] Center for Instrument Sharing University of Pisa (CISUP), Lungarno Pacinotti 43/44, 56126, Pisa, Italy.
[d.] Institute for Polymers, Composites and Biomaterials (IPCB), Italian National Research Council, Viale J.F. Kennedy 54, Mostra d'Oltremare Pad 20, 80125, Napoli, Italy.
[e.] National Interuniversity Consortium for Materials Science and Technology (INSTM), Via Giuseppe Giusti 9, 50121, Firenze, Italy.

Corresponding Authors:

Lina Altomare: lina.altomare@polimi.it;
Sivlia Borsacchi: silvia.borsacchi@pi.iccom.cnr.it

Content:

S1. Composition optimization

In this section, a composition optimization of MC hydrogels was carried out. Such an optimization study was centred on the swelling behavior and the gelation temperature of MC hydrogels prepared with a Na_2SO_4 concentration ranging from 100 to 200 mM. Based on the outcomes of this step, MC_150 (referred in the Main Text as MC) was selected as optimal for the envisioned application, and thoroughly characterized also in combination with CaP and CaPGO (MC-CaP and MC-CaPGO in the Main Text).

S1.1. Experimental

Swelling tests

The stability of the prepared gels was assessed in 1X PBS solution at 37 °C up to 28 days. At selected time points (1, 7, 14, 21, 28 days), the weight of the swollen samples (w_t) was recorded and compared with the initial weight (w_0), to calculate the swelling (SW %) of the samples according to Eq. (1):

$$SW\ (\%) = \frac{w_t - w_0}{w_0} * 100 \quad (1)$$

Tube inversion tests

Tube inversion tests were carried out by placing aliquots (10 mL) of MC hydrogels into 50 mL Falcon tubes, increasing the sample temperature from 20 to 40 °C with thermal steps of 1 °C (10 min equilibration at each temperature step), and tilting the Falcon tube by 180° at each step to evaluate the temperature (*i.e.*, T_{gel}) at which the MC gel did not flow.[1]

S1.2. Results

Swelling tests

A preliminary characterization was carried out on MC hydrogels at different Na_2SO_4 concentrations (100, 150, 200 mM), with and without the addition of CaP and CaPGO powders (1% (w/v)), to select the optimal Na_2SO_4 concentration. For the sake of simplicity, only data concerning CaP-loaded MC hydrogels (samples MC_X_CaP, with X = Na_2SO_4 mM concentration) and MC-hydrogels (samples MC_X, with X = Na_2SO_4 mM concentration) are reported in the following, since GO was found not to significantly affect swelling and gelation temperature (data not shown), as further confirmed by rheological analysis (see Main Text).

As shown in Figure S1 A, all MC_X samples undergo a rapid water uptake, reaching the swelling equilibrium within 24 h, in accordance with previous findings on similar MC hydrogel formulations.[2] Swelling (SW) values between 100 and 150 % are observed, except for the MC_100 sample, which shows SW values below 50 %. This difference can be attributed to the lower amount of dissolved salt ions. Indeed, it has been widely reported how ions (*e.g.*, SO_4^{2-}) can directly influence both the water uptake and the sol-gel transition of MC hydrogels.[3,4] Such outcomes are also confirmed in terms of stability: MC_100 is the less stable sample, dissolving faster than MC_150 and MC_200 in a water environment.

Regarding the CaP-loaded MC hydrogels, MC_100_CaP displays lower SW values at long swelling times compared with the other two formulations, undergoing complete dissolution within the end of the test (Figure S1 B). An increase in the SW values is observed on moving from MC_100_CaP to MC_150_CaP, while a further increase in Na_2SO_4 concentration (MC_200_CaP) seems to reduce the overall SW rate of the formulation. This phenomenon can be once again ascribed to the presence of salts in solution. In particular, the synergistic effect of Na_2SO_4 and CaP possibly leads to an overall salting out effect, influencing the water uptake of the hydrogels.[2] Moreover, formulation stability increases by increasing the Na_2SO_4 concentration, with MC_150_CaP and MC_200_CaP formulations resulting stable up to 28 days.

Overall, these findings revealed a good stability in an aqueous environment for both MC and MC-CaP composite hydrogels, in line with literature data on injectable hydrogels for bone tissue engineering.[5-7]

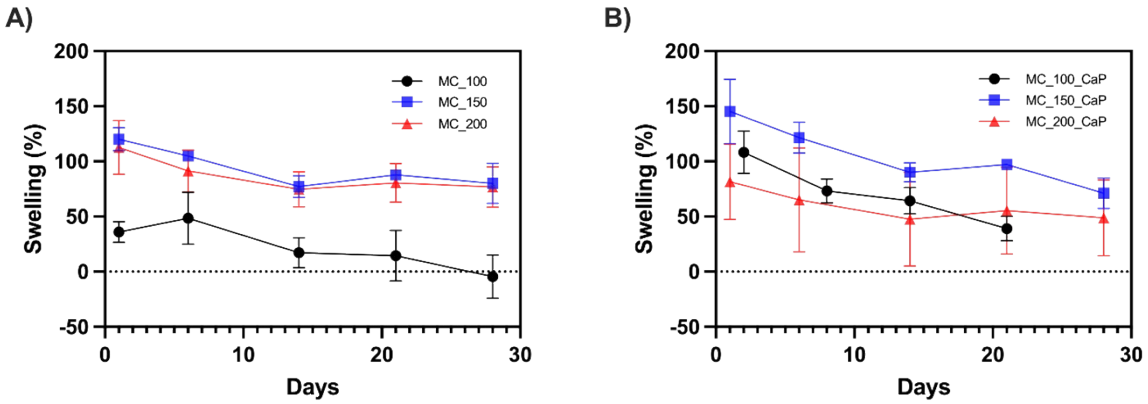

Figure S1 – Swelling tests in PBS solution at 37 °C for A) MC_X and B) MC_X_CaP formulations, where X indicates Na_2SO_4 mM concentration.

Tube inversion tests

Tube inversion tests were performed to understand the influence of Na_2SO_4 and CaP concentrations on the gelation temperature (T_{gel}) of the formulations. An increase in Na_2SO_4 concentration leads to a decrease of T_{gel} from 39 °C for MC_100 to 32 °C for MC_200. As previously reported,[8,9] Na_2SO_4 promotes the interactions among MC chains and the formation of a physical gel at lower temperatures. The addition of CaP (1 % (w/v)) results in slight or no shift of the T_{gel} of the composites, which was detected around 34 °C (as for MC_150 sample), probably due to the relatively low amount of calcium phosphates added in the gels.

S2. Characterization of hydrogels

S2.1. Experimental

FT-IR investigations

For Fourier transform infrared spectroscopy (FT-IR) experiments, the hydrogel specimens were first frozen at -20°C, then freeze-dried (-40 °C, < 0.5 mbar). FT-IR analysis was carried out on KBr disks using a Varian 640-IR spectrometer (Agilent Technologies, Santa Clara, CA, USA), in the spectral window 400-4000 cm^{-1} (4 cm^{-1} resolution, 64 scans per sample, N_2 atmosphere).

Simulated body fluid (SBF)

Mineralization tests were performed by immersing the samples in Simulated Body Fluid (SBF), prepared according to the protocol described by Kokubo et al.[10] All reagents were purchased from Merck (Merck Life Science S.r.l., Italy) and used without further purification. For 1 L of SBF solution, 0.5 L of Millipore water was heated at 37 °C in a polypropylene beaker. The reagents listed in Table S1 were then added in the order reported. 1 M HCl (reagent n° 10) was added dropwise until a pH of 7.4 was reached. Lastly, the volume of the obtained solution was brought to 1 L. The SBF solution was stored in a refrigerator (4 °C) until used.

Table S1 – SBF composition. Reagents were added in the order reported in the table.

Order of addition	Reagent	Weight/volume for 1L of SBF
1	NaCl	8.035 g
2	$NaHCO_3$	0.355 g
3	KCl	0.225 g
4	$K_2HPO_4 \cdot 3H_2O$	0.231 g
5	$MgCl_2 \cdot 6H_2O$	0.311 g
6	HCl (1M)	39 mL
7	$CaCl_2$	0.292 g
8	Na_2SO_4	0.072 g
9	Tris	6.118 g
10	HCl (1M)	0-5 mL

Rheology: amplitude sweep tests

Amplitude sweep tests were carried out on each formulation to identify the linear viscoelastic region (LVR) by applying an oscillatory strain (γ) in the 0.01 – 10 % range, setting a 1 Hz frequency (ν), at 20 and 40 °C.

S2.2. Results

FT-IR investigations

FT-IR spectroscopy was employed to examine the inclusion of CaP and CaPGO powders in the composite hydrogel. To enhance the visibility of the spectral peaks, the spectra were divided into two specific regions: 400-1000 and 1200-4000 cm^{-1}. This division was implemented to prevent the interference of Na_2SO_4 peaks at 1126 cm^{-1}, which could otherwise hinder the analysis of peaks related to the inorganic phases. Peaks due to the inorganic phases are visible in the spectra, in particular at 670, 835, 950 cm^{-1} for phosphate groups and at 1380 cm^{-1} for carbonate groups. These results showed a good integration of the powders in the gels, as underlined by the appearance of the characteristic peaks of these materials, in line with what emerges from the literature.[11,12]

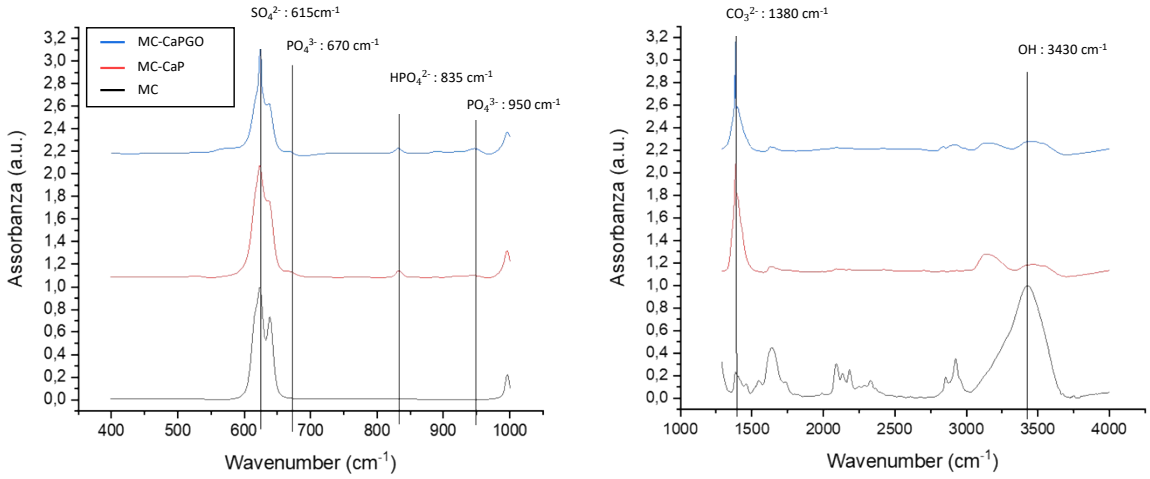

Figure S2 – FT-IR spectra of MC, MC-CaP, and MC-CaPGO formulations. For the sake of clarity, the spectra were divided in two regions: 400-1000 and 1200-4000 cm^{-1}.

Rheology: amplitude sweep tests

Shear strain tests were conducted to determine the Linear Viscoelastic Region (LVR) of the samples at two distinct temperatures, 20 and 37 °C (Figure S3). All the samples exhibit a linear viscoelastic behavior up to 10 % strain. At 20 °C, all samples display a liquid-like behavior, with loss modulus (G") higher than the storage modulus (G') for all the tested formulations. Conversely, at 37°C, a solid-like behavior can be observed, with G’ > G’’. Such a behavior indicates that the sol-gel transition of MC hydrogels, for the three formulations, occurs at temperatures between 20 and 37 °C (as already revealed from tube inversion tests, see above). The inclusion of inorganic powders in the hydrogel resulted in a slight increase of both G’ and G’’, indicating an increased gel strength.[5]

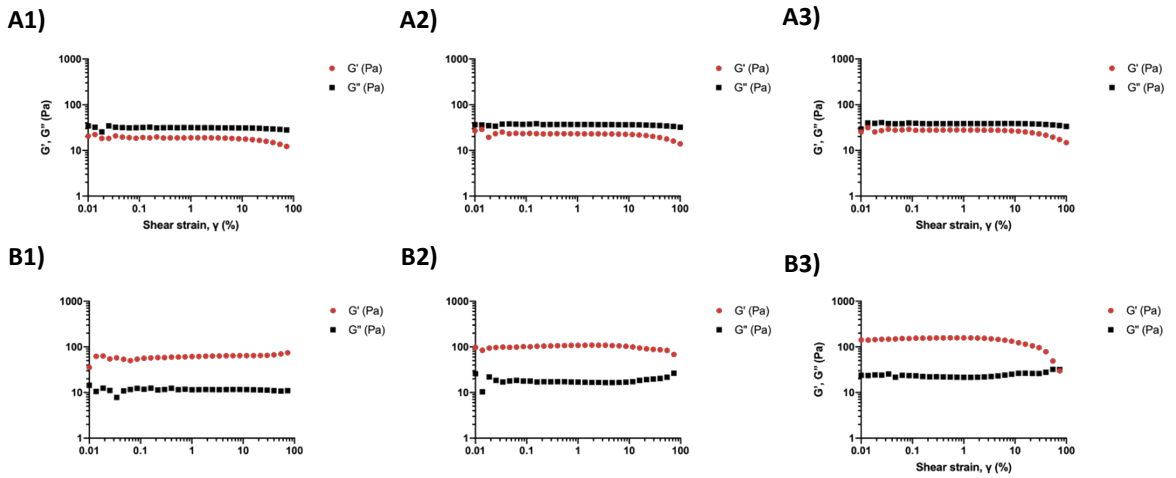

Figure S3 – Amplitude sweep tests: at 20 °C for A1) MC, A2) MC-CaP, and A3) MC-CaPGO formulations, at 37 °C for for B1) MC, B2) MC-CaP, and B3) MC-CaPGO formulations. The tests were carried by applying an oscillatory shear strain (γ) in the 0.01 – 100 range, ν = 1 Hz.

S3. Characterization of CaP and CaPGO powders

S3.1. Experimental

SSNMR measurements

SSNMR spectra were recorded on a Bruker Avance Neo spectrometer working at Larmor frequencies of 500.13, 125.77 and 202.46 MHz for ^{1}H, ^{13}C, and ^{31}P, respectively, using a triple-resonance Magic Angle Spinning (MAS) probe head accommodating rotors with an external diameter of 2.5 mm. ^{31}P Direct Excitation (DE) MAS spectra were recorded under high-power decoupling from ^{1}H nuclei, using a recycle delay of 1000 s and 600 s for CaP and CaPGO, respectively. ^{31}P Cross Polarization (CP) MAS spectra were recorded using a contact time values of 0.5 ms and a recycle delay of 10 s. ^{1}H MAS spectra were recorded with a DE pulse sequence, using a recycle delay of 80 s and 40 s for CaP and CaPGO, respectively. The ^{1}H-^{31}P HETCOR spectrum was recorded with FLSG during t1, 64 increments in the second dimension, with a dwell time of 76 µs and a contact time of 2 ms. For each increment, 16 transients were accumulated. ^{13}C DE-MAS spectra of GO and CaPGO were recorded using a recycle delay of 10 s and accumulating 400 and 31300 transients for GO and CaPGO, respectively. All spectra were recorded at a MAS frequency of 20 kHz, using air as spinning gas, at room temperature. The chemical shift scale was referenced to the signal of adamantane at 38.48 ppm for ^{13}C and calculated from the same value for all other nuclei, using the unified scale recommended by IUPAC.

S3.2. Results

A preliminary characterization of the phosphate containing phases present in the CaP and CaPGO powders was performed by ^{1}H and ^{31}P SSNMR experiments in order to establish relationships with the composition of the phases formed in the hydrogels' mineralization. Moreover, ^{13}C SSNMR was applied to investigate the GO structure in CaPGO.

In Figure S4 (A,C) quantitative ^{31}P DE-MAS NMR spectra of CaP and CaPGO are shown. The spectrum of CaP shows three main peaks at chemical shifts of -1.1, 0.5, and 3.2 ppm, which, based on the literature, can be assigned to monetite (-1.1 and 0.5 ppm)[13-15] and crystalline hydroxyapatite (3.2 ppm)[16,17]. The observation of two peaks for monetite ($CaHPO_4$) in a 1:1 integral intensity ratio arises from the presence of two inequivalent P atoms (P1 and P2) in the crystal structure.[13,15] It must be mentioned that a minor peak is present at about 1.5 ppm, which could be due to a small amount of hydrated monetite. On the other hand, hydroxyapatite ($Ca_{10}(PO_4)_6OH_2$) shows only one peak, in agreement with the presence of a sole kind of P atom in its structure. This assignment is also confirmed by the comparison between ^{31}P DE and CP-MAS spectra (Figure S4). In fact, in the CP spectrum acquired with a short contact time (0.5 ms), to allow the selective observation of P atoms spatially close to H ones, the signal of hydroxyapatite is suppressed, in agreement with its structure. On the other hand, signals of monetite are clearly observed in the CP spectrum, with a relative enhancement of the signal at 0.5 ppm, in agreement with the short distance between P2 atoms and hydroxyl hydrogen atoms (d = 2.2 Å).[13,15] From the areas underlying the signals in the ^{31}P DE-MAS spectrum, obtained through a spectral deconvolution, it is possible to quantify the relative amounts of P atoms in hydroxyapatite and monetite as 1:5.

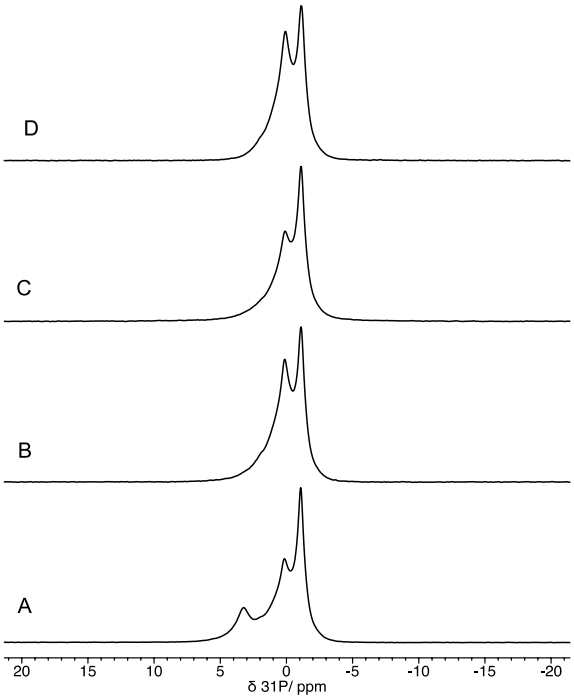

Figure S4 – ^{31}P MAS spectra of CaP (A,B) and CaPGO (C,D). Spectra A and C have been recorded with the DE pulse sequence, while B and D with the CP one.

In the ^{1}H MAS NMR spectrum of CaP (Figure S5 A), acidic hydrogens of monetite resonate at 14.1 and 16.4 ppm, in the expected intensity ratio of 1:2, and the signal of hydroxyapatite is observed at 0.45 ppm.[13,17] Moreover, a quite broad peak ascribable to water likely interacting through hydrogen-bonds with the solid is observed at 5.3 ppm, while the very narrow peak at 7.2 ppm arises from residual ammonium ions from the preparation. The very weak signal at 1.7 ppm can be ascribed to superficial -OH groups of monetite or hydroxyapatite.

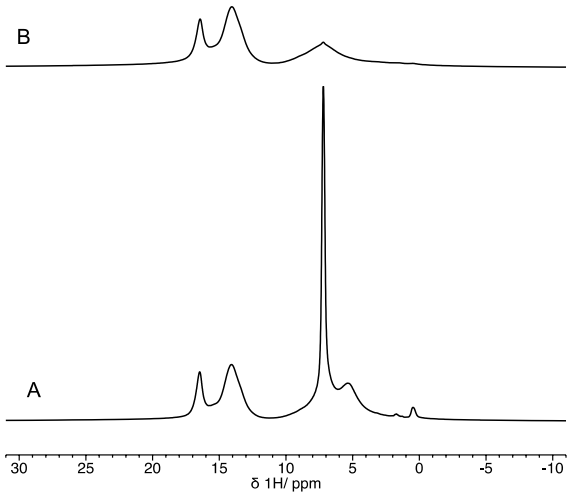

Figure S5 – ^{1}H MAS spectra of (A) CaP and (B) CaPGO.

A ^{1}H-^{31}P HETCOR MAS NMR spectrum with a short contact time was also recorded (Figure S6) in order to observe cross-peaks from spatially close ^{1}H and ^{31}P nuclei. As expected, the HETCOR spectrum shows cross-peaks between ^{31}P and ^{1}H signals of monetite, while the cross-peak between the hydroxyapatite signals is quite weak.

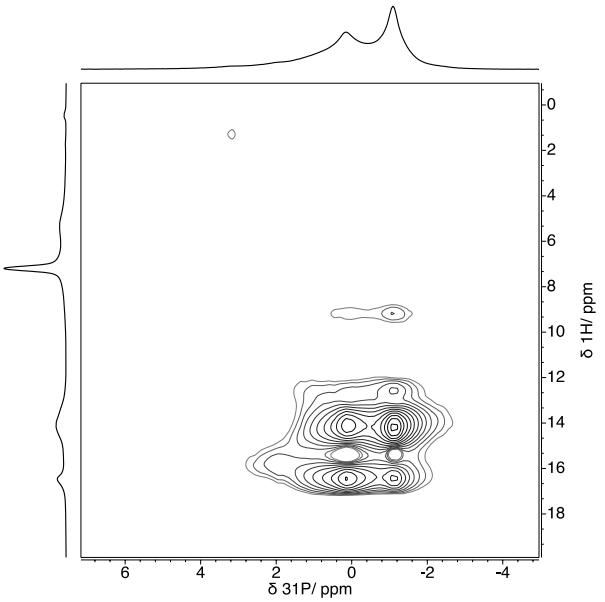

Figure S6 – ^{1}H-^{31}P HETCOR spectrum of CaP.

As far as CaPGO is concerned, in the ^{31}P DE-MAS NMR spectrum (Figure S4 B,D) only the signals of monetite are observed, while the peak at 3.2 ppm is not present, indicating that, differently from CaP, hydroxyapatite did not form in this sample. Accordingly, the ^{1}H MAS NMR spectrum of CaPGO (Figure S5 B) shows the peaks of acidic hydrogens of monetite and a broad peak ascribable to water and residual ammonium. The ^{1}H-^{31}P HETCOR MAS NMR spectrum (not reported) displays cross-peaks between ^{1}H and ^{31}P signals of monetite. These results indicate that the presence of GO prevents the formation of crystalline hydroxyapatite, and this could be related to an interaction between phosphate or calcium ions and GO.[18, 19]

Moreover, from the intensity of spectra recorded with different recycle delay values (not shown), a shortening of the spin-lattice relaxation times, T_1's, of both ^{31}P and ^{1}H nuclei is observed, which can be ascribed to the interaction between the nuclear spins and the spins of the GO unpaired electrons. This points to a good dispersion of GO in CaPGO.

We also recorded ^{13}C DE-MAS NMR spectra of GO and CaPGO (Figure S7). The ^{13}C spectrum of GO shows three main signals at about 63, 133 and 168 ppm, ascribable to C-OH/C-OR groups, aromatic moieties, and ester/carboxylic acid groups, respectively.[20-24] In the ^{13}C spectrum of CaPGO the intensity of the C-OH/OR peak decreases, while that of the ester/carboxylic peak increases, indicating a partial oxidation of GO. It must be noticed that a broad intense signal appears in the alkyl spectral region (0-50 ppm), which can be ascribed either to a reduction of GO or to impurities whose signals become visible since very many transients were accumulated.

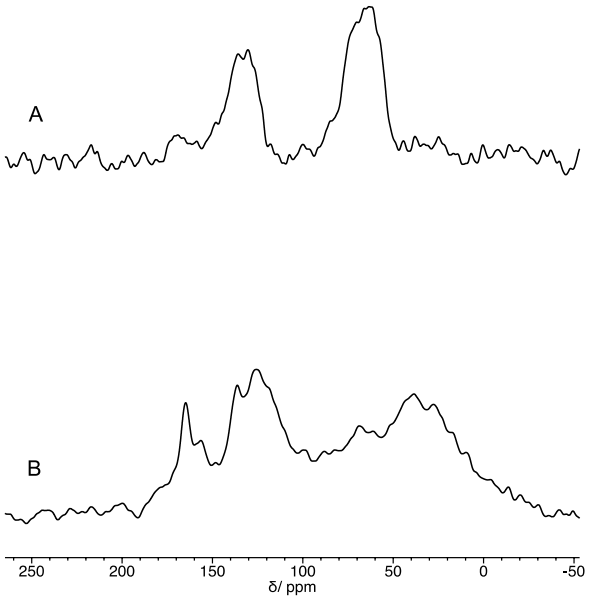

Figure S7 – ^{13}C DE-MAS NMR spectra of GO (A) and CaPGO (B).

References

1 Altomare, L., Cochis, A., Carletta, A., Rimondini, L., & Farè, S. (2016). Thermo-responsive methylcellulose hydrogels as temporary substrate for cell sheet biofabrication. *Journal of Materials Science: Materials in Medicine*, *27*, 1-13.

2 Bonetti, L., De Nardo, L., & Variola, F. (2020). Evaluation of the subtle trade-off between physical stability and thermo-responsiveness in crosslinked methylcellulose hydrogels. *Soft matter*, *16*(24), 5577-5587.

3 Bonetti, L., De Nardo, L., & Farè, S. (2021). Thermo-responsive methylcellulose hydrogels: From design to applications as smart biomaterials. *Tissue Engineering Part B: Reviews*, *27*(5), 486-513.

4 Xu, Y., Wang, C., Tam, K. C., & Li, L. (2004). Salt-assisted and salt-suppressed sol− gel transitions of methylcellulose in water. *Langmuir*, *20*(3), 646-652.

5 Fiorati, A., Linciano, C., Galante, C., Raucci, M. G., & Altomare, L. (2021). Bioactive hydrogels: Design and characterization of cellulose-derived injectable composites. *Materials*, *14*(16), 4511.

6 Durairaj, K., Balasubramanian, B., Arumugam, V. A., Easwaran, M., Park, S., Issara, U., ... & Mousavi Khaneghah, A. (2023). Biocompatibility of Veratric acid–encapsulated Chitosan/Methylcellulose Hydrogel: Biological characterization, osteogenic efficiency with in silico molecular modeling. *Applied Biochemistry and Biotechnology*, 1-18.

7 Ren, B., Chen, X., Du, S., Ma, Y., Chen, H., Yuan, G., ... & Niu, X. (2018). Injectable polysaccharide hydrogel embedded with hydroxyapatite and calcium carbonate for drug delivery and bone tissue engineering. *International journal of biological macromolecules*, *118*, 1257-1266.

8 Bonetti, L., De Nardo, L., & Farè, S. (2021). Chemically crosslinked methylcellulose substrates for cell sheet engineering. *Gels*, *7*(3), 141.

9 Cochis, A., Bonetti, L., Sorrentino, R., Contessi Negrini, N., Grassi, F., Leigheb, M., ... & Farè, S. (2018). 3D printing of thermo-responsive methylcellulose hydrogels for cell-sheet engineering. *Materials*, *11*(4), 579.

10 Kokubo, T., & Takadama, H. (2006). How useful is SBF in predicting in vivo bone bioactivity?. *Biomaterials*, *27*(15), 2907-2915.

11 Kim, M. H., Kim, B. S., Park, H., Lee, J., & Park, W. H. (2018). Injectable methylcellulose hydrogel containing calcium phosphate nanoparticles for bone regeneration. *International journal of biological macromolecules*, *109*, 57-64.

12 Park, H., Kim, M. H., Yoon, Y. I., & Park, W. H. (2017). One-pot synthesis of injectable methylcellulose hydrogel containing calcium phosphate nanoparticles. *Carbohydrate polymers*, *157*, 775-783.

13 Yu, Y., Stevensson, B., Pujari-Palmer, M., Guo, H., Engqvist, H., & Edén, M. (2019). The monetite structure probed by advanced solid-state NMR experimentation at fast magic-angle spinning. *International Journal of Molecular Sciences*, *20*(24), 6356.
14 Yu, Y., Guo, H., Pujari-Palmer, M., Stevensson, B., Grins, J., Engqvist, H., & Edén, M. (2019). Advanced solid-state 1H/31P NMR characterization of pyrophosphate-doped calcium phosphate cements for biomedical applications: The structural role of pyrophosphate. *Ceramics International*, *45*(16), 20642-20655.
15 Rothwell, W. P., Waugh, J. S., & Yesinowski, J. P. (1980). High-resolution variable-temperature phosphorus-31 NMR of solid calcium phosphates. *Journal of the American Chemical Society*, *102*(8), 2637-2643.
16 Hayakawa, S., Tsuru, K., Iida, H., Ohtsuki, C., & Osaka, A. (1996). ^{31}P MAS-NMR Studies of Phosphate Salts Formation on Calcium-Containing Oxide Glasses in a Simulated Body Fluid. *J. Ceram. Soc. Jpn.*, 104(1215), 1000–1003.
17 Mathew, R., Gunawidjaja, P. N., Izquierdo-Barba, I., Jansson, K., García, A., Arcos, D., ... & Edén, M. (2011). Solid-state 31P and 1H NMR investigations of amorphous and crystalline calcium phosphates grown biomimetically from a mesoporous bioactive glass. *The Journal of Physical Chemistry C*, *115*(42), 20572-20582.
18 Yan, L., Xu, Z., & Deng, N. (2020). Synthesis of organophosphate-functionalized graphene oxide for enhancing the flame retardancy and smoke suppression properties of transparent fire-retardant coatings. *Polymer Degradation and Stability*, *172*, 109064.
19 Verma, S., & Nadagouda, M. N. (2021). Graphene-based composites for phosphate removal. *ACS omega*, *6*(6), 4119-4125.
20 Lerf, A., He, H., Riedl, T., Forster, M., & Klinowski, J. (1997). 13C and 1H MAS NMR studies of graphite oxide and its chemically modified derivatives. *Solid State Ionics*, *101*, 857-862.
21 Wang, S., Dong, Y., He, C., Gao, Y., Jia, N., Chen, Z., & Song, W. (2017). The role of sp 2/sp 3 hybrid carbon regulation in the nonlinear optical properties of graphene oxide materials. *RSC advances*, *7*(84), 53643-53652.
22 Casabianca, L. B., Shaibat, M. A., Cai, W. W., Park, S., Piner, R., Ruoff, R. S., & Ishii, Y. (2010). NMR-based structural modeling of graphite oxide using multidimensional 13C solid-state NMR and ab initio chemical shift calculations. *Journal of the American Chemical Society*, *132*(16), 5672-5676.
23 Rawal, A., Che Man, S. H., Agarwal, V., Yao, Y., Thickett, S. C., & Zetterlund, P. B. (2021). Structural complexity of graphene oxide: the kirigami model. *ACS Applied Materials & Interfaces*, *13*(15), 18255-18263.
24 Cai, W., Piner, R. D., Stadermann, F. J., Park, S., Shaibat, M. A., Ishii, Y., ... & Ruoff, R. S. (2008). Synthesis and solid-state NMR structural characterization of 13C-labeled graphite oxide. *Science*, *321*(5897), 1815-1817.